

Article

Understanding Interfacial Reactions in Ti–Ni Diffusion Couple

Amin Babaei-Dehkordi ¹, Mansour Soltanieh ^{1,*}, Mostafa Mirjalili ², Mohammadreza Asherloo ³
and Amir Mostafaei ^{3,*}

¹ School of Metallurgy and Materials Engineering, Iran University of Science and Technology (IUST), Tehran 16846-13114, Iran; a.babaeidehkordi@gmail.com

² Department of Materials and Metallurgical Engineering, Faculty of Engineering, Ferdowsi University of Mashhad, Mashhad 91775-1111, Iran

³ Department of Mechanical, Materials and Aerospace Engineering, Illinois Institute of Technology, 10 W 32nd Street, Chicago, IL 60616, USA

* Correspondence: mansour_soltanieh@iust.ac.ir (M.S.); mostafaei@iit.edu (A.M.)

Abstract: The diffusion phenomenon in the Ti–Ni binary system was investigated at a temperature of 1173 K. Microstructure and texture analysis revealed the formation of three stable intermetallic compounds, namely Ti₂Ni, TiNi, and TiNi₃, as well as two metastable intermetallic compounds, including Ti₃Ni₄ and Ti₂Ni₃, at the interfacial diffusion zone. The nucleation surface energy increase was analytically estimated, and marker experiments were conducted using thoria particles, both of which showed that Ti₂Ni was the first compound to form at the Ti–Ni diffusion interface. At a temperature of 1173 K, using the Wagner method, the integrated diffusion coefficients for the Ti₂Ni, TiNi, and TiNi₃ phases were calculated to be 3.53×10^{-12} , 18.1×10^{-15} , and 6.2×10^{-15} m²/s, for, respectively.

Keywords: Ti–Ni system; intermetallic compounds; integrated diffusion coefficient; scanning electron microscopy



Citation: Babaei-Dehkordi, A.; Soltanieh, M.; Mirjalili, M.; Asherloo, M.; Mostafaei, A. Understanding Interfacial Reactions in Ti–Ni Diffusion Couple. *Materials* **2023**, *16*, 2267. <https://doi.org/10.3390/ma16062267>

Academic Editors: Renhai Shi, Lijun Zhang and Ying Tang

Received: 12 February 2023

Revised: 5 March 2023

Accepted: 7 March 2023

Published: 11 March 2023



Copyright: © 2023 by the authors. Licensee MDPI, Basel, Switzerland. This article is an open access article distributed under the terms and conditions of the Creative Commons Attribution (CC BY) license (<https://creativecommons.org/licenses/by/4.0/>).

1. Introduction

Ti–Ni alloys, known for their exceptional properties such as shape memory effect, corrosion resistance, shock absorption, superelasticity, and biocompatibility, have found applications in diverse fields ranging from aerospace, automotive, and oil to biomedical sectors [1–4]. Given their importance, ongoing research in the field of the Ti–Ni binary system is focused on exploring its potential applications [5–8]. Depending on the heat treatment conditions, the Ti–Ni binary system can produce three stable intermetallic compounds, namely Ti₂Ni, TiNi, and TiNi₃, as well as two metastable intermetallic compounds, Ti₃Ni₄ and Ti₂Ni₃ [9]. However, limited attention has been given to the diffusion coefficients of alloying elements, which significantly affect the kinetics of intermetallic compound formation [1,10–15].

In the Ti–Ni binary system, TiNi is the most important compound, and its formation is influenced by the two other stable phases, Ti₂Ni and TiNi₃. Therefore, understanding the sequence and formation mechanism of TiNi is crucial. A diffusion couple study is a practical approach to investigate diffusion phenomena in solid-state conditions. The formation of different intermetallic compounds in the Ti–Ni binary system is based on diffusional transformation, including the metastable phases of Ti₃Ni₄ → Ti₂Ni₃ → TiNi₃ (stable), where temperature and holding duration are critical factors that determine the kinetics of this process [16].

The presence of metastable phases such as Ti₃Ni₄ and Ti₂Ni₃ in Ti–Ni alloys can affect their shape memory behavior [17–20]. However, in earlier studies investigating the formation of different intermetallic compounds in the Ti–Ni binary system using diffusion coupling, the formation of these metastable phases was disregarded [21–25]. The diffusion

coefficient of elements plays a critical role in the kinetics of diffusion during the solid-state formation of intermetallic compounds, influencing the diffusion mechanism and the sequence of intermetallic compound formation. The kinetics of growth are governed by volume diffusion and interdiffusion coefficients, which can effectively compare growth rates between different intermetallic phases [26].

Previous studies have overlooked the formation of Ti_3Ni_4 and Ti_2Ni_3 metastable intermetallic compounds in the Ti–Ni binary system. Therefore, the primary objective of this study is to investigate the formation of these metastable compounds using the integrated diffusion coefficient of elements. In this research, both experimental and analytical analyses were conducted to gain a comprehensive understanding of the formation of various intermetallic compounds in the Ti–Ni binary system.

2. Materials and Methods

To investigate the interfacial reactions and formation sequence of various phases and intermetallic compounds at the Ti–Ni diffusion couple interface, high purity commercial Ni (1 mm thick) and Ti (2 mm thick) sheets were purchased. A Ti sheet was placed between two Ni plates to form the diffusion couple. The sheets were sliced to dimensions of 15 mm × 6 mm and their surfaces were ground using SiC sandpaper up to 2500 grit. To minimize the presence of any oxide film or potential contaminations at the Ni–Ti–Ni interfaces, the metal sheets were ultrasonically etched in a mixed acidic solution consisting of 10% HCl, 67% HNO₃, and 23% deionized water. The sheets were then rinsed in acetone and dried. To ensure maximum surface contact at the Ni–Ti–Ni interfaces, a steel fixture was used. The annealing treatment was conducted in a tube furnace at a temperature of 1173 ± 5 K under an Ar atmosphere. The quartz tube was vacuumed and then backfilled with ultra-high purity Ar gas (99.999% purity) to minimize oxidation.

The microstructure at the interface of the Ti–Ni binary system was studied using a standard metallographic procedure, which included a final polishing step of 0.05 μm colloidal silica. The morphology, composition, and thickness of the formed intermetallic compounds at the Ti–Ni interface were analyzed using a scanning electron microscope (SEM, TESCAN VEGA//XMU) equipped with an energy-dispersive spectrometer (EDS). The morphological structure of the Ti sheet was observed using an optical microscope (MEIJI TECHNO, MT7350, Japan). Texture and phase analyses were performed using a JEOL JSM 5900-LV SEM equipped with an Oxford Instruments Nordlys Nano electron backscatter diffraction (EBSD) detector. The EBSD imaging was conducted at an accelerating voltage of 20 keV, and the data were analyzed using Channel 5-HKL software.

3. Results and Discussion

Figure 1a shows SEM images of the Ti–Ni interface, which appears fairly straight, suggesting uniform pressure on the flat surfaces. Elemental analysis revealed that the layer adjacent to the Ti sheet had a composition of 68.9 at% Ti and 31.1 at% Ni, indicating the dominant formation of a Ti_2Ni intermetallic phase after annealing at 1173 K for 13 h. Two narrow intermetallic layers were also detected near the Ni side, with the TiNi layer composed of 50.6 at% Ti and 49.4 at% Ni, and the TiNi_3 layer adjacent to the Ni sheet containing an elemental fraction of 26.3 at% Ti and 73.7 at% Ni. These observations are consistent with the Ti–Ni binary diagram and previous studies [21–23,25,27–29]. The Ti_2Ni layer was thicker than the TiNi and TiNi_3 layers and had an island microstructure. To analyze the crystal structure of the three intermetallic compounds and investigate the nucleation mechanism and growth behavior at the Ti–Ni interface, EBSD analysis was performed. The results in Figure 1b show the presence of two additional intermetallic compounds, Ti_3Ni_4 and Ti_2Ni_3 , at the Ti–Ni interface in addition to the Ti_2Ni , TiNi, and TiNi_3 intermetallic compounds. Ti_3Ni_4 and Ti_2Ni_3 are identified as metastable phases in the Ti–Ni phase diagram [30].

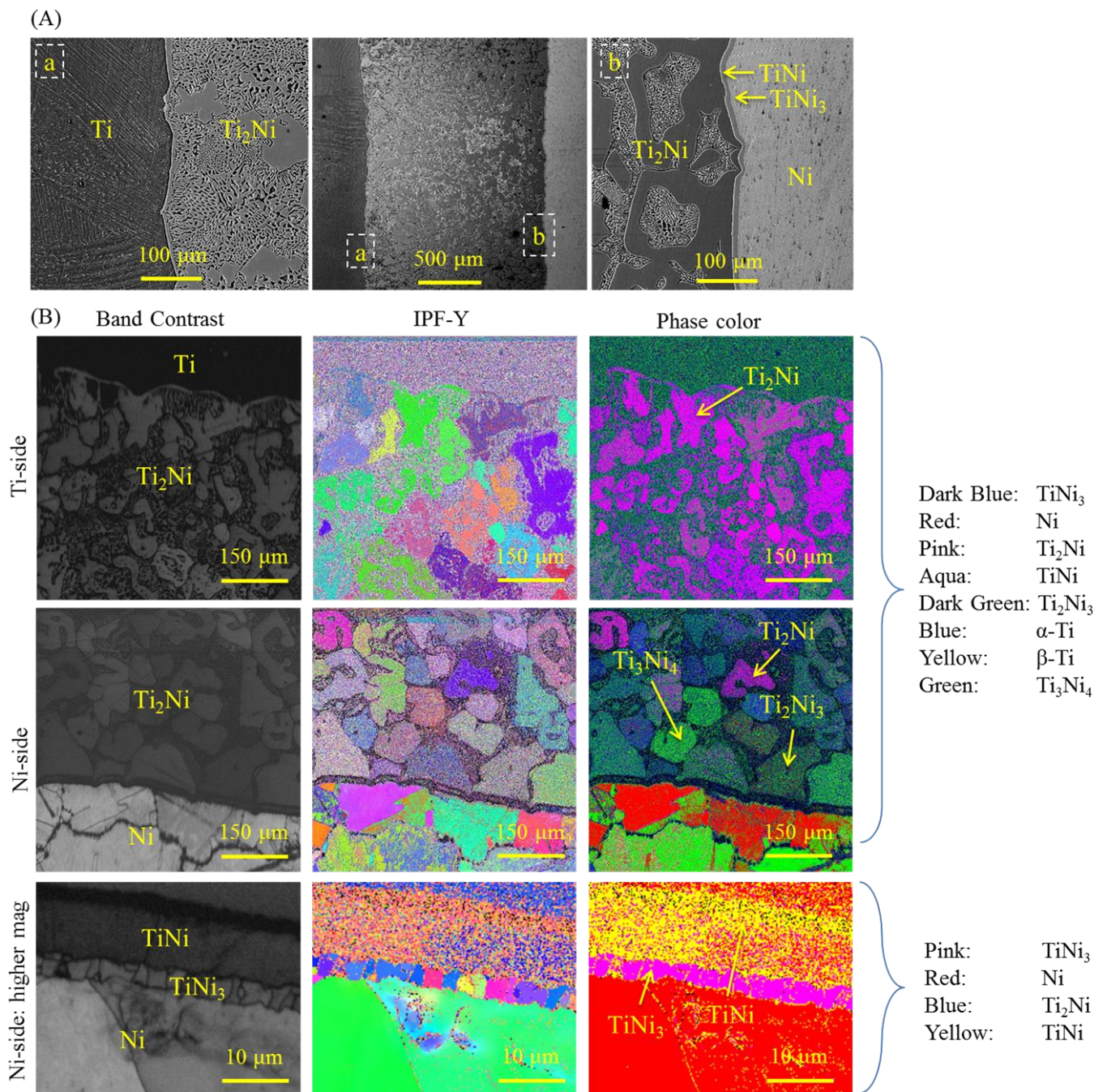


Figure 1. (A) SEM micrographs from the Ti–Ni diffusion couple annealed at 1173 K for 13 h (etched by Kroll’s reagent). (B) Electron backscattered diffraction from the Ti–Ni interface.

The grain size distribution in the diffusion layers was observed in the EBSD results (Figure 1b) taken from both the Ti and Ni sides. Fine-grained Ti_2Ni was formed close to the Ti side, while coarse mixed grains were formed on the Ni side. The unindexed areas close to the Ti side were attributed to the fine-grained structure of the Ti alloy. To elucidate the formation mechanism, it is crucial to identify the dominant diffusing element, determine the diffusion coefficients of the elements, and investigate the first intermetallic layer formed at the Ti–Ni binary system. The sequence of intermetallic compound formation at the Ti–Ni interface can be determined by calculating the Gibbs free energies of formation for the three compounds as a function of temperature [25].

The formation of intermetallic compounds in the Ti–Ni binary system is a complex process that is governed by kinetics. Although the calculation of Gibbs free energy is important, it alone is not sufficient to determine the order of intermetallic formation. The formation process involves a series of events such as the diffusion of Ni and Ti, formation of saturated primary solid solutions, nucleation, and growth of an equilibrium phase in a sequential manner. When all the necessary conditions are met, a new phase will be formed at the interface of Ti–Ni.

In the Ti–Ni binary system, the interdiffusion phenomenon leads to the formation of saturated solid solutions of Ti (Ni) and Ni (Ti) on either side. The lower solubility limit of Ni in Ti at the annealing temperature resulted in the formation of the Ti (Ni) solid solution and nucleation of the Ti₂Ni phase. According to nucleation theory, a compound with the lowest interfacial energy will nucleate more easily than other compounds at the diffusion zone [31].

The determination of the increasing interfacial energy involves several factors, including the interfacial energy of the initial *A/B* interface (γ_{A-B} , *A* or *B* can be either Ti or Ni), the surface energy of the *AB* phase (γ_{AB} , where *AB* can be Ti₂Ni, Ti₃Ni₄, Ti₂Ni₃, TiNi, or TiNi₃), the surface energy of the initial substances (γ_i , where *i* = Ti or Ni) and the interfacial energy of the new interface *AB/A* or *AB/B* (γ_{A-AB} or γ_{B-AB}). These terms can be calculated using the following equations [32,33]:

$$\gamma_{A-B} = \frac{1}{6} (\gamma_A + \gamma_B) + \frac{\Delta H_{A \text{ in } B}^{interface}}{C_0 V_A^{2/3}} \quad (1)$$

$$\gamma_{AB} = C_A^S \gamma_A + C_B^S \gamma_B - C_A^S C_B^S \frac{\Delta H_{A \text{ in } B}^{interface}}{C_0 V_A^{2/3}} \quad (2)$$

$$\gamma_{A-AB} = \frac{1}{6} (\gamma_A + \gamma_{AB}) + \frac{C_B^S \Delta H_{A \text{ in } B}^{interface}}{C_0 V_A^{2/3}} \quad (3)$$

$$\Delta H_{A \text{ in } B}^{interface} = \frac{2PV_A^{2/3}}{n_A^{-1/3} + n_B^{-1/3}} [-(\phi_A - \phi_B)^2 + \frac{Q \left(n_A^{1/3} - n_B^{1/3} \right)^2}{P} - \frac{R}{P}] \quad (4)$$

$$C_A^S = C_A V_A^{2/3} / \left(C_A V_A^{2/3} + C_B V_B^{2/3} \right) \quad (5)$$

$$C_B^S = C_B V_B^{2/3} / \left(C_A V_A^{2/3} + C_B V_B^{2/3} \right) \quad (6)$$

where $\Delta H_{A \text{ in } B}^{interface}$ is the enthalpy change upon the solution of 1 mole of *A* in *B*, V_A is the molar volume of Ti or Ni atoms ($V_{Ti} = 10.6 \text{ cm}^3/\text{mol}$, $V_{Ni} = 6.54 \text{ cm}^3/\text{mol}$) [33], C_0 is a constant, taken as 4.5×10^8 [31], C_A and C_B are the concentrations of *A* and *B* atoms, respectively, γ_A is the surface energy ($\gamma_{Ni} = 2000 \text{ mJ}/\text{m}^2$, $\gamma_{Ti} = 2051 \text{ mJ}/\text{m}^2$), n_i is the electron density ($n_{Ti}^{1/3} = 1.47$, $n_{Ni}^{1/3} = 1.75$). $\frac{Q}{P}$, $\frac{R}{P}$ and P are constant values and are equal to 9.4, 1.9, and 12.35, respectively [33]. C_A^S and C_B^S are the surface fraction of *A* and *B* atoms [31]. Based on Equations (1)–(6), the γ_{Ti-Ni} is $-106.37 \text{ mJ}/\text{m}^2$ and the increasing interface energies of Ti₂Ni, Ti₃Ni₄, Ti₂Ni₃, TiNi, and TiNi₃ compounds is calculated and listed in Table 1. The formation of Ti₂Ni, Ti₃Ni₄, Ti₂Ni₃, TiNi, and TiNi₃ compounds is associated with a 647.5, 891, 686.1, 674.1, and a 692.2 mJ/m^2 increase in interface energy, respectively. Based on the results, it can be inferred that the formation of Ti₂Ni has the lowest interface energy, suggesting that Ti₂Ni nucleates first in the Ti–Ni diffusion couple.

Table 1. The increasing interface energies of different first formation phases.

Phases	Surface Energy γ (AB) (mJ/m ²)	Interface Energy γ (Ti-AB) (mJ/m ²)	Interface Energy γ (Ni-AB) (mJ/m ²)	Increasing Interface Energy (mJ/m ²)
Ti ₃ Ni ₄	2222.4	328.8	455.7	891.0
Ti ₂ Ni ₃	2220.6	305.0	274.6	686.1
TiNi ₃	2185.1	169.6	416.3	692.2
Ti ₂ Ni	2191.2	498.0	42.8	647.5
TiNi	2220.9	382.5	185.4	674.1

In this study, the marker test was used to determine the predominant diffusing element by placing ThO₂ particles at the Ti–Ni interface. As ThO₂ particles act as a marker for the true position of the Kirkendall plane [34], their location revealed the diffusing element. Figure 2 shows the location of the ThO₂ particles at the Ni/Ni₃Ti interface. According to EDS results, the first layer adjacent to the Ti side contained 68.5 at% Ti and 31.5 at% Ni, while the next layer contained 51.3 at% Ti and 49.7 at% Ni. The layer adjacent to the Ni side contained 26.3 at% Ti and 73.7 at% Ni, indicating the formation of Ti₂Ni, TiNi, and TiNi₃, respectively.

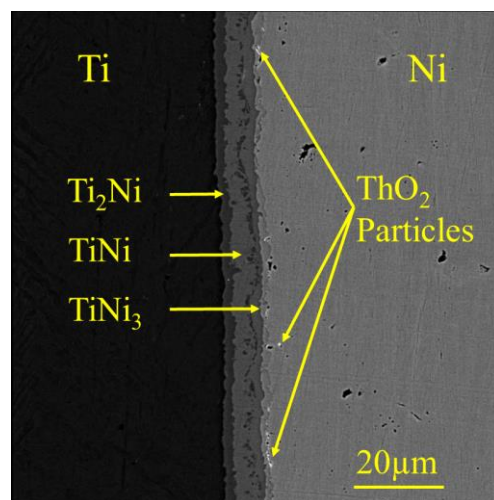


Figure 2. SEM micrograph at the interface of the Ti–Ni diffusion couple. To study the diffusion behavior, ThO₂ particles were placed at the Ti–Ni interface. The sample was annealed at 1173 K for 5 h.

In the Ti–Ni binary system, the ratio of intrinsic diffusivities can be determined at the location of the Kirkendall marker plane using the following Equation (7) [35,36]:

$$\frac{V_{Ti}D_{Ni}}{V_{Ni}D_{Ti}} = \frac{D_{Ni}^*}{D_{Ti}^*} = \frac{N_{Ni}^+ \int_{x^-}^{x_k} (N_{Ni} - N_{Ni}^-) dx - N_{Ni}^- \int_{x_k}^{x^+} (N_{Ni}^+ - N_{Ni}) dx}{-N_{Ti}^+ \int_{x^-}^{x_k} (N_{Ni} - N_{Ni}^-) dx \mp N_{Ti}^- \int_{x_k}^{x^+} (N_{Ni}^+ - N_{Ni}) dx} \quad (7)$$

where D_i is the intrinsic diffusion coefficient, D_i^* is the tracer diffusion coefficient, V_i is the partial molar volume of element i , x_k is the Kirkendall marker plane location, and x^- and x^+ correspond to the unaffected ends of the diffusion couple [37]. Due to the position of the marker location at the Ni/TiNi₃ interface, it can be concluded that $\frac{D_{Ni}^*}{D_{Ti}^*} = \infty$, meaning that Ni was the dominant diffusing element in the Ni–Ti diffusion couple. These observations are consistent with the analytical calculations of the increasing interface energy of the intermetallic phases in the Ti–Ni interface, as described by Equations (1)–(6).

Based on the EDS results, the layer formed between the Ti and Ni sheets in Figure 3a contains 66.4 at% Ti and 33.6 at% Ni, which is most likely due to the formation of Ti₂Ni.

Similarly, the layer formed on the Ti side in Figure 3b contains 67 at% Ti and 33 at% Ni, while the next layer contains 23 at% Ti and 77 at% Ni, indicating the formation of Ti_2Ni and TiNi_3 , respectively. These results suggest that the Ti_2Ni intermetallic compound is the first phase formed at the interface of the Ti–Ni diffusion couple. These observations are supported by numerical calculations and marker experiments.

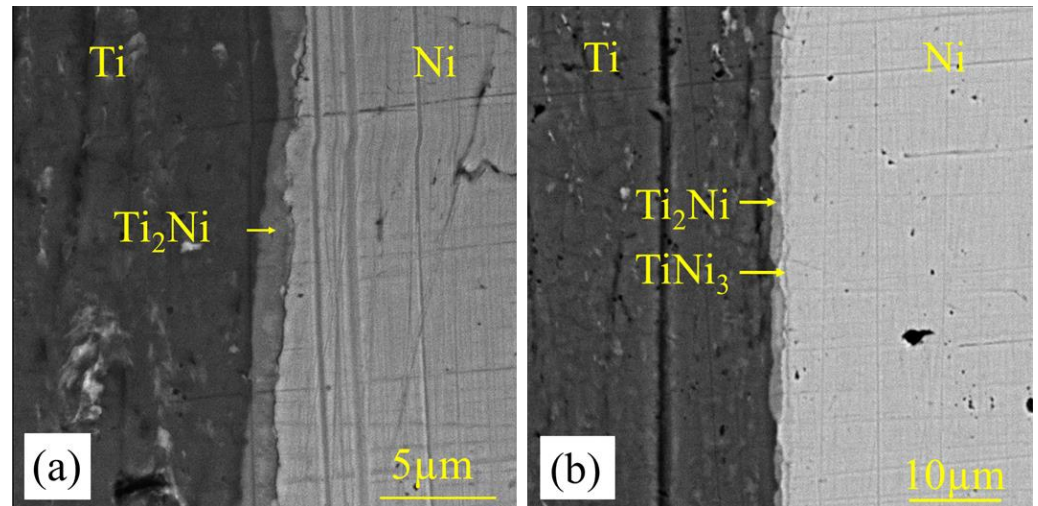
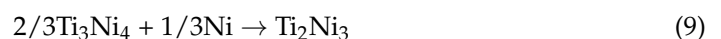


Figure 3. SEM micrographs at the interface of the Ti–Ni diffusion couple annealed at 900 °C for (a) 1 min and (b) 5 min.

After formation of the Ti_2Ni layer, two new interfaces, namely Ti/ Ti_2Ni and $\text{Ti}_2\text{Ni}/\text{Ni}$, are formed. These interfaces differ from the original Ti/Ni interface and cannot be described by Equations (1)–(6). Previous studies have reported the formation of three main intermetallic compounds, including Ti_2Ni , TiNi , and TiNi_3 [21–23], while the formation of metastable phases such as Ti_3Ni_4 and Ti_2Ni_3 has been overlooked. Due to the higher diffusion rate of Ni toward Ti [24], a saturated solid solution of Ti (Ni) is formed, and a fine Ti_2Ni phase is nucleated near the Ti side, as shown in Figure 1a. With prolonged annealing treatment, grain coarsening occurs in the Ti_2Ni layer close to the Ti side. The Ni continues to diffuse through this layer, and the metastable phase Ti_3Ni_4 is formed according to the following equation:



Excessive diffusion of Ni can result in the formation of another metastable phase including Ti_2Ni_3 , according to the following equation:



Subsequently, as shown in Figure 3b, the stable TiNi_3 intermetallic compound was formed on the Ni side according to the following equation:



Finally, a stable TiNi phase was formed in the interface of the Ti_2Ni and TiNi_3 layers, as shown in Figure 3b, according to the following equation:



The subsequent formation and growth of the intermetallic layers are affected by the diffusion of Ti and Ni elements through the formed layers. After the formation of a continuous TiNi layer at the $\text{Ti}_2\text{Ni}/\text{TiNi}_3$ interface, the $\text{Ti}_2\text{Ni}/\text{TiNi}_3$ interface disappeared, and new interfaces were formed, including $\text{TiNi}/\text{TiNi}_3$ and $\text{Ti}_2\text{Ni}/\text{TiNi}$. Therefore, the formation and growth of the TiNi layer can be explained by two other reactions instead

of Equation (11). To determine the subsequent growth of the intermetallic layers, it is necessary to identify the dominant diffusing element.

Based on the marker experiment, it can be inferred that Ni is the predominant diffusing element in the Ti–Ni binary system due to its lower melting temperature and smaller atomic radius (1728 K, 163 pm) compared with Ti (1941 K, 187 pm) [38]. As a result, faster diffusion of the Ni element through the formed layers at the Ti/Ti₂Ni interface can potentially form a fine-grained structure of Ti₂Ni. As per Equation (12), a portion of the diffused Ni reacts with Ti₂Ni at the Ti₂Ni/TiNi interface, leading to the formation of the TiNi layer. The dissolution of Ti₂Ni grains and their conversion to TiNi grains lead to the formation of a dendrite-like structure at the Ti₂Ni/TiNi interface in accordance with previous studies [21,36].



At the TiNi/TiNi₃ interface, part of the diffused Ti through the Ti₂Ni and TiNi layers reacts with the TiNi₃ intermetallic compound, forming and growing the TiNi layer, as given in Equation (13).



It should be noted that the formation rate of the TiNi₃ layer is expected to be lower than that of the Ti₂Ni layer due to the higher diffusivity of Ni. Moreover, the accumulation of vacancies at the TiNi₃/Ni interface decreases the diffusion of Ni over a prolonged annealing time, and the TiNi₃ layer acts as an Ni source. Finally, the lower formation of the TiNi₃ layer compared with the consumption of this layer results in the consumption of the TiNi₃ layer, which is in agreement with other results [28].

The diffusion coefficient of elements is a key factor to determining the sequence formation of phases and growth mechanism in the Ti–Ni diffusion couples. The Wagner equation [39,40] (Equation (14)) can be used to calculate the diffusion coefficient in a multi-component structure:

$$\tilde{D}_{int}^{\beta} = \frac{(N_i^{\beta} - N_i^{-}) (N_i^{+} - N_i^{\beta})}{N_i^{+} - N_i^{-}} \frac{\Delta x_{\beta}^2}{2t} + \frac{\Delta x_{\beta}}{2t} \left[\frac{(N_i^{+} - N_i^{\beta}) \sum_{v=2}^{v=\beta-1} \frac{V_m^{\beta}}{V_m^v} (N_i^v - N_i^{-}) \Delta x_v + (N_i^{\beta} - N_i^{-}) \sum_{v=\beta+1}^{v=n-1} \frac{V_m^{\beta}}{V_m^v} (N_i^{+} - N_i^v) \Delta x_v}{N_i^{+} - N_i^{-}} \right] \quad (14)$$

where \tilde{D}_{int}^{β} (m²/s) is the integrated diffusion coefficient, N_i^{-} and N_i^{+} are the mole fractions of component i in the unreacted left- and right-hand sides of the ends of the couple, respectively. N_i^{β} and N_i^v are the mole fractions of component i in the phase of interest β and v , respectively, V_m^v and Δx_v are the molar volume and the layer thickness of the v phase, and t is the annealing time. The data used to calculate the integrated diffusion coefficients of the Ti₂Ni, TiNi, and TiNi₃ phases formed in the Ti–Ni diffusion couple after annealing at 1173 K for 13 h are represented in Table 2. Based on Equation (14), the integrated diffusion coefficients for the Ti₂Ni, TiNi, and TiNi₃ phases were 3.53×10^{-12} , 18.1×10^{-15} , and 6.2×10^{-15} m²/s, respectively.

Table 2. Experimental data after annealing of Ti–Ni diffusion couple for 13 h at 1173 K.

Phase, j	Ti	Ti ₂ Ni	TiNi	TiNi ₃	Ni
Thickness, μm	-	1391	11	6	-
Ni Mole fraction, N _{Ni}	0.03	0.32	0.49	0.74	1
Ti Mole fraction, N _{Ti}	0.97	0.68	0.51	0.26	0
Molar volume (V _j , cm ³)	-	9	8.2	7	-

The integrated diffusion coefficient calculated in this study is not consistent with the results presented in [40], which showed that the integrated diffusion coefficient is higher in the Ti_2Ni layer. Grain boundaries play an important role in accelerating the diffusion phenomena, as they act as fast diffusion paths and promote formation of intermetallic layers [26]. The activation energy for grain boundary diffusion is about half that for lattice diffusion [41], and the grain boundary diffusion coefficient (D_{gb}) is much greater than the diffusion coefficient in bulk (D_l). Diffusion is faster in fine-grained solids; thus, the mass transport process is affected by the grain size of the polycrystalline material [42].

In this research, a Ti sheet was used as received without any pre-annealing process, unlike our earlier study [40], in which an annealed titanium sheet (at 1023 K for 3 h holding time) was used. As shown in Figure 4, the higher integrated diffusion coefficient in Ti_2Ni could be attributed to the finer structure of the titanium used. Moreover, the Ti has a bcc crystal structure at 1173 K with a lower packing factor (PF) compared with the hcp crystal structure at lower temperatures (<1155 K). Therefore, it is expected that the Ti_2Ni layer forms faster than the other intermetallic layers, and the integrated diffusion coefficient is greater in this layer than the other layers, in agreement with the calculation results. Using finer-grained Ti is expected to result in the formation of intermetallic layers at a shorter annealing time. Hence, the difference in the diffusion coefficient value could be related to the difference in the grain size of the primary sheets.

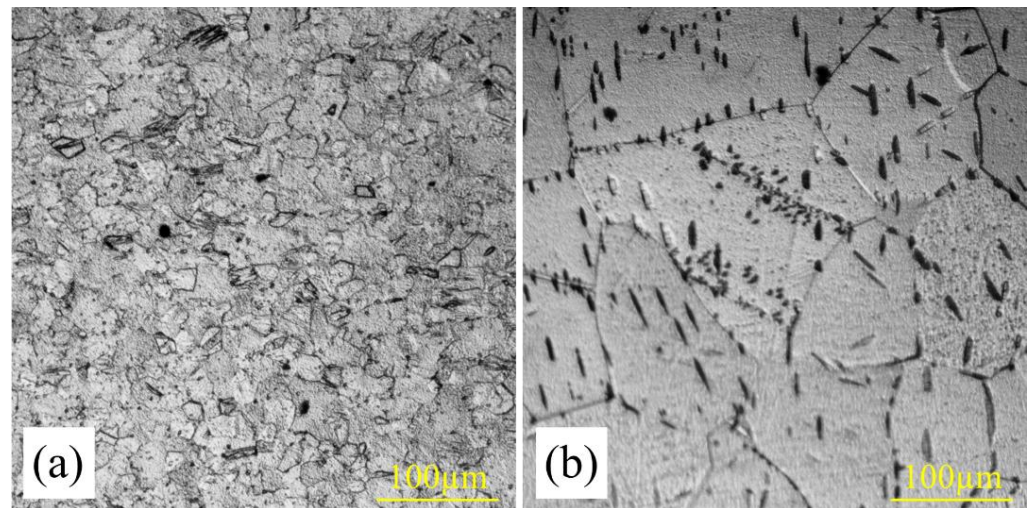


Figure 4. Optical micrograph of the cross-section of Ti sheet (a) as received without any pre-annealing process and (b) annealed at 1033 K for 150 min.

4. Conclusions

The diffusion phenomenon in the Ti–Ni binary system was investigated at 1173 K. It was found that:

1. Three intermetallic compounds in the sequence of Ti_2Ni , $TiNi$, and $TiNi_3$ and two metastable intermetallic compounds including Ti_3Ni_4 and Ti_2Ni_3 were formed at the Ti–Ni interface.
2. The marker technique and calculating the ratio of intrinsic diffusivities indicated that Ni is the dominant diffusing element.
3. The integrated diffusion coefficients, calculated using the Wagner method, were 3.53×10^{-12} , 18.1×10^{-15} , and 6.2×10^{-15} m^2/s for Ti_2Ni , $TiNi$, and $TiNi_3$ at 1173 K, respectively.
4. Annealing of the titanium sheet resulted in grain growth, which reduced the contribution of grain boundaries to the overall diffusion and resulted in the reduction. As a result, the integrated diffusion coefficient in the Ti_2Ni layer decreased.

Author Contributions: Methodology, A.B.-D. and M.M.; Validation, A.M.; Formal analysis, A.B.-D. and M.A.; Investigation, A.B.-D.; Resources, M.S. and A.M.; Writing—original draft, A.B.-D.; Writing—review & editing, M.S. and A.M.; Visualization, A.B.-D. and M.A.; Supervision, M.S. and A.M.; Funding acquisition, A.M. All authors have read and agreed to the published version of the manuscript.

Funding: This research was funded, in part, by National Science Foundation grant number DMR-2050916 and the APC was covered by Prof. Amir Mostafaei.

Institutional Review Board Statement: Not applicable.

Informed Consent Statement: Not applicable.

Data Availability Statement: Data will be made available on request.

Acknowledgments: A.M. acknowledges startup funding from the Mechanical, Materials and Aerospace Engineering Department at the Illinois Institute of Technology in Chicago, Illinois. A.M. acknowledges partial support from the National Science Foundation under grant number DMR-2050916.

Conflicts of Interest: The authors declare that they have no known competing financial interest or personal relationships that could have appeared to influence the work reported in this paper.

References

1. Kim, A.; Makhmutov, T.; Razumov, N.; Silin, A.; Popovich, A.; Zhu, J.-N.; Popovich, V. Synthesis of NiTi alloy powders for powder-based additive manufacturing. *Mater. Today Proc.* **2020**, *30*, 679–682. [[CrossRef](#)]
2. y Puente, A.P.; Dunand, D. Synthesis of NiTi microtubes via the Kirkendall effect during interdiffusion of Ti-coated Ni wires. *Intermetallics* **2018**, *92*, 42–48. [[CrossRef](#)]
3. Shi, Q.; Zhang, Y.; Tan, C.; Mao, X.; Khanlari, K.; Liu, X. Preparation of Ni–Ti composite powder using radio frequency plasma spheroidization and its laser powder bed fusion densification. *Intermetallics* **2021**, *136*, 107273. [[CrossRef](#)]
4. Zou, P.; Zheng, C.; Hu, L.; Wang, H. Rapid Growth of TiNi intermetallic compound within undercooled Ti50Ni50 alloy under electrostatic levitation condition. *J. Mater. Sci. Technol.* **2021**, *77*, 82–89. [[CrossRef](#)]
5. Bai, X.; Cai, Q.; Xie, W.; Zeng, Y.; Chu, C.; Zhang, X. In-situ crystalline TiNi thin films deposited by HiPIMS at a low substrate temperature. *Surf. Coat. Technol.* **2023**, *455*, 129196. [[CrossRef](#)]
6. Wu, F.; Chen, H.; Yang, Z.; Qiao, J.; Hou, Y.; Yan, R.; Bai, H. Investigation on the electronic structures, elastic and thermodynamic properties of TiNi, Ti₂Ni and TiNi₃ intermetallic compound. *Mater. Today Commun.* **2023**, *34*, 105273. [[CrossRef](#)]
7. Sampath, S.; Vedamanickam, S. Effect of Vanadium on the Microstructure, Transformation Temperatures, and Corrosion Behavior of NiTi Shape Memory Alloys. *J. Eng. Mater. Technol.* **2023**, *145*, 011008. [[CrossRef](#)]
8. Balasubramanian, C.; Rajkumar, K.; Santosh, S. Enhancement of machining and surface quality of quaternary alloyed NiTiCuZr shape memory alloy through ultrasonic vibration coupled WEDM. *Proc. Inst. Mech. Eng. Part L J. Mater. Des. Appl.* **2022**, *236*, 816–833. [[CrossRef](#)]
9. Parvizi, S.; Hashemi, S.M.; Moein, S. 19—NiTi shape memory alloys: Properties. In *Nickel-Titanium Smart Hybrid Materials*; Thomas, S., Behera, A., Nguyen, T.A., Eds.; Elsevier: Amsterdam, The Netherlands, 2022; pp. 399–426. [[CrossRef](#)]
10. Senthilkumar, V.; Velmurugan, C. Spark Plasma Sintering of NiTi Shape Memory Alloy. In *Spark Plasma Sintering of Materials*; Springer: Berlin/Heidelberg, Germany, 2019; pp. 635–670.
11. Vojtěch, D.; Michalcová, A.; Čapek, J.; Marek, I.; Dragounová, L. Structural and mechanical stability of the nano-crystalline Ni–Ti (50.9 at.% Ni) shape memory alloy during short-term heat treatments. *Intermetallics* **2014**, *49*, 7–13. [[CrossRef](#)]
12. Tajdari, M.; Mehraban, A.G.; Khoogar, A. Shear strength prediction of Ni–Ti alloys manufactured by powder metallurgy using fuzzy rule-based model. *Mater. Des.* **2010**, *31*, 1180–1185. [[CrossRef](#)]
13. Tomochika, H.; Kikuchi, H.; Araki, T.; Nishida, M. Fabrication of NiTi intermetallic compound by a reactive gas laser atomization process. *Mater. Sci. Eng. A* **2003**, *356*, 122–129. [[CrossRef](#)]
14. Petrović, S.; Peruško, D.; Mitrić, M.; Kovac, J.; Dražić, G.; Gaković, B.; Homewood, K.P.; Milosavljević, M. Formation of intermetallic phase in Ni/Ti multilayer structure by ion implantation and thermal annealing. *Intermetallics* **2012**, *25*, 27–33. [[CrossRef](#)]
15. Salvetr, P.; Kubatík, T.F.; Pignol, D.; Novák, P. Fabrication of Ni-Ti alloy by self-propagating high-temperature synthesis and spark plasma sintering technique. *Metall. Mater. Trans. B* **2017**, *48*, 772–778. [[CrossRef](#)]
16. Lang, P.; Wojcik, T.; Povoden-Karadeniz, E.; Cirstea, C.D.; Kozeschnik, E. Crystal structure and free energy of Ti₂Ni₃ precipitates in Ti–Ni alloys from first principles. *Comput. Mater. Sci.* **2014**, *93*, 46–49. [[CrossRef](#)]
17. Miyazaki, S.; Otsuka, K. Deformation and transition behavior associated with the R-phase in Ti–Ni alloys. *Metall. Trans. A* **1986**, *17*, 53–63. [[CrossRef](#)]
18. Nishida, M.; Honma, T. All-round shape memory effect in Ni-rich TiNi alloys generated by constrained aging. *Scr. Metall.* **1984**, *18*, 1293–1298. [[CrossRef](#)]
19. Xie, C.; Zhao, L.; Lei, T. Effect of Ti₃Ni₄ precipitates on the phase transitions in an aged Ti–51.8 at% Ni shape memory alloy. *Scr. Metall. Mater.* **1990**, *24*, 1753–1758. [[CrossRef](#)]

20. Nomura, K.; Miyazaki, S.; Takei, A. Transformation and deformation behavior of sputter deposited Ti-Ni thin films. In *Ecomaterials*; Elsevier: Amsterdam, The Netherlands, 1994; pp. 1049–1052.
21. Bastin, G.; Rieck, G. Diffusion in the titanium-nickel system: I. occurrence and growth of the various intermetallic compounds. *Metall. Trans.* **1974**, *5*, 1817–1826. [[CrossRef](#)]
22. Garay, J.; Anselmi-Tamburini, U.; Munir, Z.A. Enhanced growth of intermetallic phases in the Ni-Ti system by current effects. *Acta Mater.* **2003**, *51*, 4487–4495. [[CrossRef](#)]
23. Zhou, Y.; Wang, Q.; Sun, D.; Han, X. Co-effect of heat and direct current on growth of intermetallic layers at the interface of Ti-Ni diffusion couples. *J. Alloys Compd.* **2011**, *509*, 1201–1205. [[CrossRef](#)]
24. Hinotani, S.; Ohmori, Y. The microstructure of diffusion-bonded Ti/Ni interface. *Trans. Jpn. Inst. Met.* **1988**, *29*, 116–124. [[CrossRef](#)]
25. Hu, L.; Xue, Y.; Shi, F. Intermetallic formation and mechanical properties of Ni-Ti diffusion couples. *Mater. Des.* **2017**, *130*, 175–182. [[CrossRef](#)]
26. Wang, L.; Wang, Y.; Prangnell, P.; Robson, J. Modeling of intermetallic compounds growth between dissimilar metals. *Metall. Mater. Trans. A* **2015**, *46*, 4106–4114. [[CrossRef](#)]
27. Li, R.; Niu, P.; Deng, S.; Yuan, T.; Liu, G. Diffusivity of Ti-Ni Diffusion Couple Enhanced by Pulse Current During Spark Plasma Sintering. *Metall. Mater. Trans. B* **2020**, *51*, 6–10. [[CrossRef](#)]
28. Shao, X.; Guo, X.; Han, Y.; Lin, Z.; Qin, J.; Lu, W.; Zhang, D. Preparation of TiNi films by diffusion technology and the study of the formation sequence of the intermetallics in Ti-Ni systems. *J. Mater. Res.* **2014**, *29*, 2707–2716. [[CrossRef](#)]
29. Zhou, Y.; Yang, G.; Wu, X.; Li, C. Formation characteristics of Ni/Ti intermetallics through annealing of layered Ni/Ti. *Trans. China Weld. Inst.* **2010**, *31*, 41–44.
30. Otsuka, K.; Ren, X. Physical metallurgy of Ti-Ni-based shape memory alloys. *Prog. Mater. Sci.* **2005**, *50*, 511–678. [[CrossRef](#)]
31. Liu, J.; Su, Y.; Xu, Y.; Luo, L.; Guo, J.; Fu, H. First phase selection in solid Ti/Al diffusion couple. *Rare Met. Mater. Eng.* **2011**, *40*, 753–756. [[CrossRef](#)]
32. Benedictus, R.; Böttger, A.; Mittemeijer, E. Thermodynamic model for solid-state amorphization in binary systems at interfaces and grain boundaries. *Phys. Rev. B* **1996**, *54*, 9109. [[CrossRef](#)]
33. Miedema, A.; De Chatel, P.; De Boer, F. Cohesion in alloys—Fundamentals of a semi-empirical model. *Phys. B+C* **1980**, *100*, 1–28. [[CrossRef](#)]
34. Van Loo, F. Multiphase diffusion in binary and ternary solid-state systems. *Prog. Solid State Chem.* **1990**, *20*, 47–99. [[CrossRef](#)]
35. Paul, A.; Laurila, T.; Vuorinen, V.; Divinski, S.V. *Thermodynamics, Diffusion and the Kirkendall Effect in Solids*; Springer: Berlin/Heidelberg, Germany, 2014.
36. Paul, A.; Divinski, S. Diffusion Fundamentals and Techniques. In *Handbook of Solid State Diffusion*; Elsevier: Amsterdam, The Netherlands, 2017; Volume 1.
37. Buscaglia, V.; Anselmi-Tamburini, U. On the diffusional growth of compounds with narrow homogeneity range in multiphase binary systems. *Acta Mater.* **2002**, *50*, 525–535. [[CrossRef](#)]
38. Dybkov, V.I. Regularities of Reactive Diffusion and Phase Formation in Ni—Bi, Ni—Zn, and Co—Zn Binary Systems. *Powder Metall. Met. Ceram.* **2001**, *40*, 426–431. [[CrossRef](#)]
39. Wagner, C. The evaluation of data obtained with diffusion couples of binary single-phase and multiphase systems. *Acta Metall.* **1969**, *17*, 99–107. [[CrossRef](#)]
40. Babaei-Dehkordi, A.; Soltanieh, M.; Mirjalili, M.; Mostafaei, A. Quantitative analysis of diffusion kinetics of intermetallic formation in Ni-Ti system. *J. Mater. Res. Technol.* **2022**, *20*, 4545–4555. [[CrossRef](#)]
41. Brennan, S.; Bermudez, K.; Kulkarni, N.S.; Sohn, Y. Interdiffusion in the Mg-Al system and intrinsic diffusion in β -Mg₂Al₃. *Metall. Mater. Trans. A* **2012**, *43*, 4043–4052. [[CrossRef](#)]
42. Jaseliunaite, J.; Galdikas, A. Kinetic modeling of grain boundary diffusion: The influence of grain size and surface processes. *Materials* **2020**, *13*, 1051. [[CrossRef](#)] [[PubMed](#)]

Disclaimer/Publisher's Note: The statements, opinions and data contained in all publications are solely those of the individual author(s) and contributor(s) and not of MDPI and/or the editor(s). MDPI and/or the editor(s) disclaim responsibility for any injury to people or property resulting from any ideas, methods, instructions or products referred to in the content.